PERGAMON

International Journal of Solids and Structures 40 (2003) 2449–2471

INTERNATIONAL JOURNAL OF SOLIDS and STRUCTURES

www.elsevier.com/locate/ijsolstr

Closed-loop based detection of debonding of piezoelectric actuator patches in controlled beams

Dongchang Sun, Liyong Tong *

School of Aerospace, Mechanical and Mechatronic Engineering, University of Sydney, Sydney, NSW 2006, Australia

Received 18 May 2002; received in revised form 6 January 2003

Abstract

A practical closed loop control based damage detection scheme is presented aiming at detecting small damage in controlled structures. In this detection method, a deliberately designed sensitive control system is used to augment small frequency shifts caused by small structural damage. Since a small frequency change can destabilize such a sensitive control system, it can be easily observed and thus the small damage can be detected. To perform active control of structures, a modal velocity observer (MVO) is designed by combining two observers, which can be used for multi-mode control. By properly choosing the parameters in the MVO, it can be made very sensitive to the frequency shift suitable for small damage detection. To demonstrate this method in detecting small debonding of piezoelectric patches on a smart beam, a detailed model of beam with partly debonded piezoelectric patches is established based on the Timoshenko's beam theory, in which both transverse and longitudinal vibrations are modeled, and a characteristic equation is also derived to examine the effect of the debonding on the control performance. Both the model and the control law are validated by an active vibration control experiment. Finally, an example is given to illustrate application of the method in piezoelectric actuator debonding detection. The results show that even a small edge debonding in a piezoelectric actuator patch can make the sensitive control system unstable, and therefore can be detected.

Keywords: Damage detection; Closed-loop control; Piezoelectric transducers; Debonding

1. Introduction

Investigation of damage detection in structures using piezoelectric sensors is widely conducted in recent years. Many detection methods are based on monitoring the change in modal parameters such as modal frequencies, mode shapes and modal damping ratios. As one of smart materials, piezoelectric sensors are increasingly used for health monitoring and on-line detection of delamination in composite structures, and various detection methods have been developed (see e.g. Islam and Cralg, 1994; Beard and Chang, 1997; Jian et al., 1997; Xiao et al., 2001; Fukunaga et al., 2002). Zou et al. (2000) gave a detailed review on vibration-based model-dependent damage detection for composite structures.

* Corresponding author. Fax: +61-2-93514841.
E-mail address: ltong@aeromech.usyd.edu.au (L. Tong).

0020-7683/03/$ - see front matter © 2003 Elsevier Science Ltd. All rights reserved.
doi:10.1016/S0020-7683(03)00080-5

With the emergence of new piezoelectric materials with higher performance, the piezoelectric actuator can generate large strain and sustain high actuating voltage. Although new piezoelectric materials can improve the efficiency of active control of smart structures, they also increase the possibility of debonding of the actuator from its host structure. Seeley and Chattopadhyay (1999) studied the issue of the piezoelectric actuator debonding in a composite beam by using the finite element method (FEM) based on a refined higher order theory, and found that length of debonding is a key factor to its effects on dynamic behavior. When the debonding length is small, the change of modal shapes was not noticeable. Tylikowski (2001) presented a bending-extensional model of a simply supported laminated beam with debonded piezoelectric actuator elements, and he reported that no remarkable frequency shifts were observed due to small actuator debonding. Tong et al. (2001) developed a model of beams with partially debonded piezoelectric sensors/actuators including adhesive layers, and analyzed effects of debonding on sensing and actuating behaviors. Sun et al. (2001) investigated actuator debonding on closed-loop control and found that controlled structures are more vulnerable to debonding and actuator/sensor debonding can significantly reduce the control efficiency. Therefore, it is important to find such debonding in its early stage in controlled structures.

Modal frequency changes caused by damage are one of the most important features used in damage detection, and information about changes in mode shapes or strain modes is usually employed to localize damage. However, for the controlled structures, the change in modal characteristics due to debonding of actuators may be very small because the piezoelectric actuator patches are much smaller than the host structure. When debonding of the piezoelectric patches is small, frequency change of the whole structure due to debonding can also be very small (Sun et al., 2001) and it is difficult to detect using open-loop detection schemes.

To detect a small damage in a structure, closed-loop based damage detection methods may be used to enhance the sensitivity of the modal characteristics to the damage in the structure. A deliberately designed sensitive closed-loop control system may be able to detect small damage in a controlled structure, which will not increase the cost of damage detection, since existing sensors and actuators on the controlled structures can be employed. However, very limited papers on active damage detection are available in the literature. Ray and Tian (1999) introduced a concept of enhancing modal frequency sensitivity to damage using feedback control. The concept is demonstrated for a single-degree-of-freedom structure as well as a finite-element model of a cantilevered beam. Their simulation results show that the controlled modes by a full-state feedback controller are more sensitive to changes in structural parameters than the uncontrolled ones. Recently, they also experimentally demonstrated sensitivity enhancing control used in damage detection in smart structures (Ray et al., 2000).

It is well known that the control system in a controlled structure is usually designed to control its several lowest modes since the information relevant to these modes is measured or observed much more easily than that of higher modes. However, the controlled modes with higher order are more sensitive to debonding of the actuator in a controlled structure. Therefore, the damage effects on the lowest several modes should be amplified through active control using certain control laws.

This paper aims to detect the frequency change due to small debonding of piezoelectric actuator patches in a controlled structure by a sensitive control system. A closed-loop control based detection scheme is presented to detect debonding of a piezoelectric actuator patch from its host structure. In order to detect debonding of the actuator patches from the host structure, a modal velocity observer (MVO) is designed by combining two second order observers to observe the modal velocities, and modal control is performed by feeding back the observed modal velocities. By choosing parameters, the MVOs can be made very sensitive to small frequency shift due to changes in parameters of the composite structure. Therefore, small damage levels in such a controlled structures may significantly alter the properties of the closed loop control and may even destabilized the control system, and as a result, the small damage can be easily detected. To detect debonding of actuator patches, a detailed model of a beam with partly debonded piezoelectric patches is

established based on the Timoshenko's beam theory, in which both transverse and longitudinal vibration are considered and adhesive layers are also taken into account. In addition, continuity conditions are imposed at the interfaces between the debonded and bonded regions to ensure displacement continuity and force equilibrium. A characteristic equation of the controlled beam is derived. The eigenvalues of the characteristic equation for the beam controlled by the sensitive control law are used to examine the effects of actuator debonding on the closed loop system. The detection scheme is demonstrated both theoretically and experimentally by detecting a small actuator debonding.

2. Modal velocity observer design for detection

To detect the damage in a controlled structure, a deliberately sensitized controller should be designed. First, the controller should be able to control the undamaged structures efficiently, and second, it should be made very sensitive to the changes in the structure by adjusting its parameters. It is known that damages in a structure will change its modal characteristics such as modal frequencies, modal shapes and modal damping ratios to some extent. Therefore, modal control of structures is reasonable to amplify the changes of these modal characteristics for each mode of the structure due to the damage. The existing designing methods (Lee and Moon, 1990; Sun et al., 1999; Sun and Tong, 2001) of modal sensors may not be easy to be implemented in practice at the presence of structural damage. In this section, a practical MVO is designed which can be used to estimate the designated modal velocity from the sensor output.

The charge output $q(t)$ of a piezoelectric sensor patch in a structure is proportional to the average strain in the area it covers. According to the superposition principle, the charge output of a sensor is the weighted sum of all modal displacements, i.e.

$$q(t) = \sum_{i=1}^{\infty} \alpha_i \eta_i(t) \tag{1}$$

where $\eta_i(t)$ is the ith modal displacement, α_i is the coefficient related to the locations and sizes of the sensor elements and the modal functions of the structures.

In order to extract a single modal velocity $\dot{\eta}_i(t)$ whose modal frequency is ω_i, two observers are employed as follows. The first observer is designed as

$$y_{1,tt}(t) + 2\omega_{c1}\zeta_{c1}y_{1,t}(t) + \omega_{c1}^2 y_1(t) = \omega_{c1}^2 q(t) \tag{2}$$

where ω_{c1} and ζ_{c1} are natural frequency and damping ratio of this observer respectively. Eq. (2) is a second-order observer, which functions as a low pass filter. The output $y_1(t)$ of Eq. (2) contains only the components whose frequencies are close to or less than ω_{c1}. Therefore, in positive position feedback method, this observer is employed to control the lowest mode of a structure (Sun and Tong, 2001). However, observer (2) cannot be used to observe a single mode except the first mode.

The second observer is designed as

$$y_{2,tt}(t) + 2\omega_{c2}\zeta_{c2}y_{2,t}(t) + \omega_{c2}^2 y_2(t) = \omega_{c2}y_{1,t}(t) \tag{3}$$

where ω_{c2} and ζ_{c2} are the natural frequency and damping ratio of the second observer respectively. Note that the input of the second observer is the velocity output of the first observer.

In order to examine the frequency response of the observers to the input $q(t)$, derive the complex frequency response as

$$H(\omega) = \frac{I\omega/\omega_{c2}}{[1-(\omega/\omega_{c1})^2 + I2\zeta_{c1}\omega/\omega_{c1}][1-(\omega/\omega_{c2})^2 + I2\zeta_{c2}\omega/\omega_{c2}]} \tag{4}$$

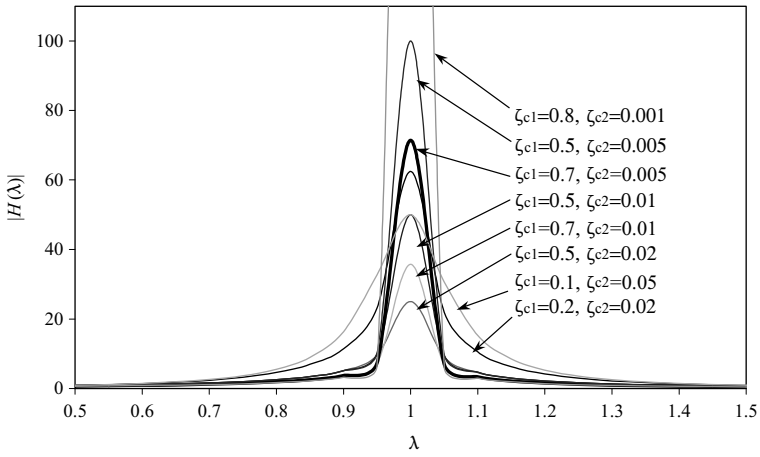

Fig. 1. Magnification factor versus frequency ratio with different damping ratios.

where ω is frequency parameter and $I = \sqrt{-1}$. Since the observers aim to extract a single mode from the sensed signal, in the following sections, ω_{c1} and ω_{c2} are always taken the same value and denoted them by ω_c, i.e. $\omega_{c1} = \omega_{c2} = \omega_c$. Denoting $\lambda = \omega/\omega_c$, the magnification factor $|H(\lambda)|$ and phase angle θ become

$$|H(\lambda)| = \frac{\lambda}{\sqrt{[(1-\lambda^2)^2 - 4\zeta_{c1}\zeta_{c2}\lambda]^2 + [2(\zeta_{c1}+\zeta_{c2})\lambda(1-\lambda^2)]^2}}$$
$$\theta(\lambda) = \tan^{-1}\frac{(1-\lambda^2)^2 - 4\zeta_{c1}\zeta_{c2}\lambda^2}{2(\zeta_{c1}+\zeta_{c2})(\lambda^3-\lambda)} \tag{5}$$

Fig. 1 is the plot of magnification factor $|H(\lambda)|$ versus frequency ratio λ with different damping ratios in the observers. As shown in Fig. 1, the magnification factor has a peak value near $\lambda = 1$, whereas it approaches zero as the frequency ratio λ is much less or larger than 1. Therefore, the combined observer in Eqs. (2) and (3) can be used as a single MVO by making its natural frequency ω_c equal to one of the frequencies of the structures. In this case, only the component with the selected frequency can pass the observer and other modal information will be suppressed in the output of the observers. It can also be noted that the damping ratios in the observers have significant effects on the sensitive bandwidth. By properly adjusting the damping ratios ζ_{c1} and ζ_{c2}, the sensitive bandwidth can be made very narrow which means that only those components whose frequencies are very close to ω_c will be found in the output. For example, when $\zeta_{c1} = 0.7$ and $\zeta_{c2} = 0.005$, the component with frequency ω_c is amplified by 71 times, but the amplifier factor for those whose frequencies are less than 95% of ω_c or greater than 105% of ω_c is less than 6.5. This means that the components with frequency far away from ω_c will be filtered out by the combined observers.

To examine the phase difference between the output $y_2(t)$ and the input $q(t)$, the phase angle θ versus frequency ratio λ is plotted in Fig. 2 with different damping ratios. As shown in Fig. 2, the phase angle is $\pi/2$ when $\lambda = 1$. In this case, the phase difference between y_2 and $q(t)$ is 90°, and $y_2(t)$ is 180° out of phase with the current $q_{,t}(t)$. It is clear that the combined observer can observe one of the modal velocities from the charge output $q(t)$ of a piezoelectric sensor patch when its frequency is chosen to be equal to this modal frequency, as shown in Fig. 2.

It is well known that the phase shift of the feedback signal affects closed-loop control much more significantly than its amplitude change. Since our purpose is to design a sensitive controller in order to sense

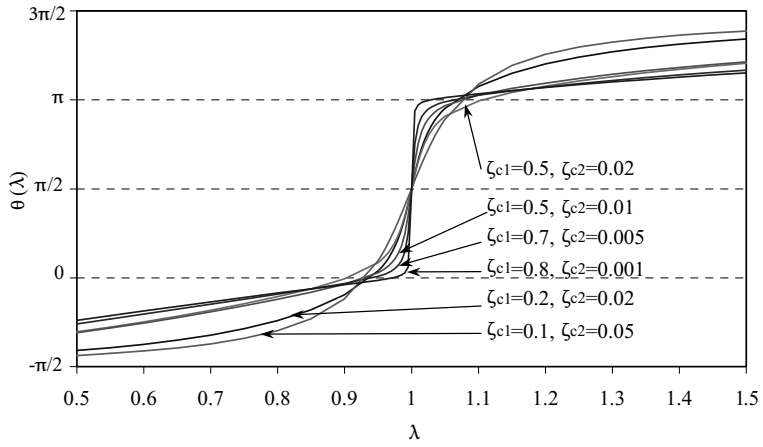

Fig. 2. Phase angle versus frequency ratio with different damping ratios.

small debonding of actuator patches, the phase angle in the neighborhood of $\lambda = 1$ is particularly interesting and plotted in Fig. 3. Fig. 3 shows that the phase angle can be made very sensitive to the frequency change of the controlled structures by assigning very small damping ratios ζ_{c1} and ζ_{c2}. For instance, when $\zeta_{c1} = \zeta_{c2} = 0.01$, a 1% change of the frequency will lead to a 100% change of the phase angle. Such a dramatic change of phase angle caused by a small frequency change will destabilize the active control. In such a way, the closed loop control system can be made very sensitive to the frequency change for the purpose of detecting small damages.

In conclusion, the combined observers in Eqs. (2) and (3) form a MVO that can extract the designed modal velocities from the charge output of a piezoelectric sensor patch. The output of the MVO can be used to provide the structures active damping by the following control law:

$$V(t) = g y_2(t) \tag{6}$$

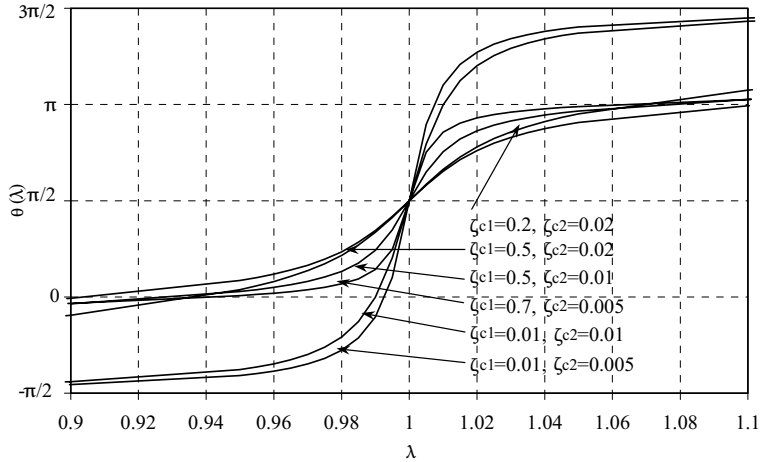

Fig. 3. Phase angle in the neighborhood of resonance.

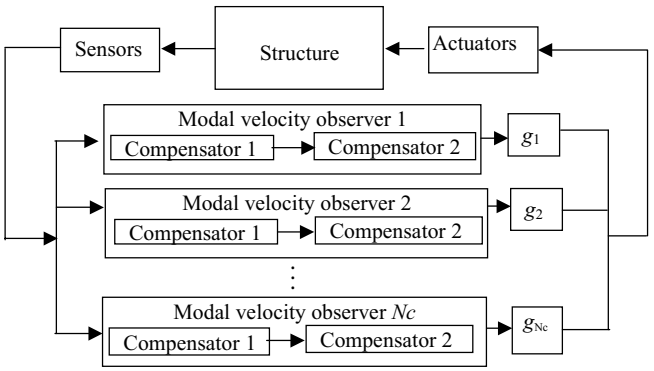

Fig. 4. Block diagram of the control process using MVO.

where $V(t)$ is the control voltage to be applied on the piezoelectric actuator and g is a control gain. If N_c modes are to be controlled simultaneously, N_c MVOs are needed and the control voltage can be obtained by

$$V(t) = \sum_{i=1}^{N_c} g_i y_{2i}(t) \tag{7}$$

where g_i is the control gain for the ith mode, and $y_{2i}(t)$ is the output of the ith MVO. The multi-mode control loop is schematically depicted in Fig. 4.

3. Mathematical model of beam with debonded actuator/sensor patches

Consider a slender composite beam with length L, on which several piezoelectric patch pairs are bonded onto its upper and lower surfaces as actuator and sensor respectively, as shown in Fig. 5. In the following derivation, assume that all debondings occur throughout the width of the beam and the debonding front lines are straight and perpendicular to the x-axis. The adhesive layers are assumed to carry constant transverse shear and peel strains due to their very thin thickness. In the debonded region, it is assumed that there is no stress transferring between the host beam and piezoelectric actuator or sensor layer. Since the debonded part of the actuator at the early stage is very small, the classical beam theory cannot accurately describe the vibration of the short debonded actuator part. Therefore, the Timoshenko's beam theory is employed. In addition, contact and friction between the two debonded surfaces are assumed to be negligible due to the small size of actuator debonding.

For the portion of the host beam covered with piezoelectric patches on its upper and lower surfaces (AB and CD portions), employing the Timoshenko's beam theory, the equations of motion can be derived as follows:

$$\begin{aligned}
&\rho_1 b h_1 u_{1,tt} = T_{1,x} + b\tau_1, \quad \rho_1 b h_1 w_{1,tt} = Q_{1,x} + b\sigma_1, \quad \rho_1 J_1 \psi_{1,tt} = M_{1,x} + b\tau_1 h_1/2 - Q_1 \\
&\rho_2 b h_2 u_{2,tt} = T_{2,x} - b\tau_1 + b\tau_2, \quad \rho_2 b h_2 w_{2,tt} = Q_{2,x} - b\sigma_1 + b\sigma_2 \\
&\rho_2 J_2 \psi_{2,tt} = M_{2,x} + b(\tau_1 + \tau_2) h_2/2 - Q_2, \quad \rho_3 b h_3 u_{3,tt} = T_{3,x} - b\tau_2 \\
&\rho_3 b h_3 w_{3,tt} = Q_{3,x} - b\sigma_2, \quad \rho_3 J_3 \psi_{3,tt} = M_{3,x} + b\tau_2 h_3/2 - Q_3
\end{aligned} \tag{8}$$

where the subscripts 1, 2 and 3 represent the upper piezoelectric layer, the host beam and the lower piezoelectric layer respectively, u and w are the longitudinal and transverse displacements, h is the thickness, b is the width of the composite beam, τ_1 and σ_1, τ_2 and σ_2 are shear and peel stresses of the upper and lower

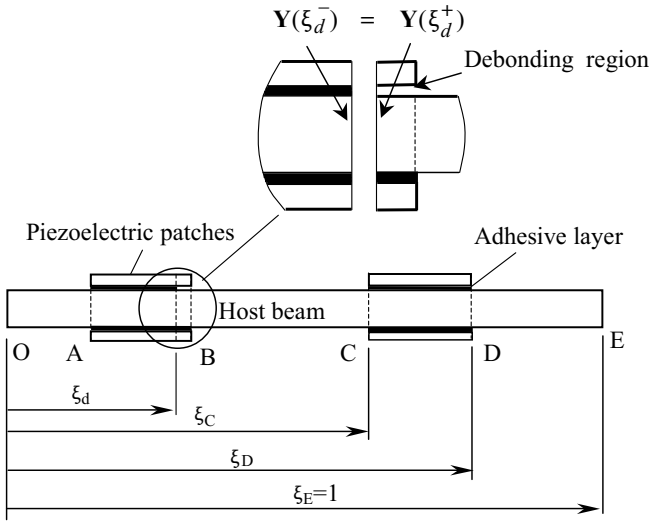

Fig. 5. Beam with partially debonded piezoelectric actuator/sensor patches: (a) detailed view of the debonding region, (b) panoramic view.

adhesive layers respectively, T, Q and M are the stress and moment resultants respectively, ρ is the equivalent mass densities, ψ is the rotation angle of the line element originally perpendicular to the longitudinal axis, which is given by

$$\psi_i = \gamma_i - w_{i,x} \quad i = 1,2,3 \tag{9}$$

and γ_i is the shear strain at the neutral axis and has the form

$$\gamma_i = \frac{c_i Q_i}{G_i A_i}, \quad i = 1,2,3 \tag{10}$$

The c_i in Eq. (10) is a constant depending on shape of the cross section. For a rectangular cross section, $c_i = 1.2$.

The stress resultants and bending moments in Eq. (8) can be derived as follows:

$$\begin{aligned} T_1 &= E_1 b h_1 u_{1,x} - b e_{311} V(t), \quad M_1 = \frac{E_1 b h_1^3}{12}\psi_{1,x} \\ T_2 &= E_2 b h_2 u_{2,x}, \quad M_2 = \frac{E_2 b h_2^3}{12}\psi_{2,x} \\ T_3 &= E_3 b h_3 u_{3,x} - b e_{311} V(t), \quad M_3 = \frac{E_3 b h_3^3}{12}\psi_{3,x} \end{aligned} \tag{11}$$

where $V(t)$ is the uniformly distributed voltage applied on the actuator, E is the Young's modulus, e_{311} is the piezoelectric stress constant of the actuator layer. Using the constant shear and peel strain assumption, the shear and peel stresses in the adhesive layer are given by

$$\begin{aligned} \tau_i &= k_1 \frac{G_{vi}}{h_{vi}}[u_{i+1} - u_i - (h_i\psi_i + h_{i+1}\psi_{i+1})/2] \\ \sigma_i &= \frac{k_i E_{vi}(1-\nu_{vi})}{(1-2\nu_{vi})(1+\nu_{vi})h_{vi}}(w_{i+1} - w_i) \quad i = 1,2 \end{aligned} \tag{12}$$

where the subscript v represents the adhesive layers, v is the Poisson's ratio, and k is a parameter describing the bonding condition

$$k_i = \begin{cases} 0 & \text{debonding} \\ 1 & \text{perfect bonding} \end{cases} \quad i = 1, 2 \tag{13}$$

Eq. (13) indicates that the peel and shear stresses in the adhesive layer are zero in the debonded regions.

When the piezoelectric patch is used as a sensor, there is no external voltage applied on it (i.e. $V(t) = 0$), and the electric charge due to the direct piezoelectric effect can be used to measure the vibration of the composite beam. If the piezoelectric patch bonded on the lower surface between C and D (see Fig. 5) used as a sensor, its charge output can be evaluated by

$$q(t) = \int_{x_C}^{x_D} be_{313} u_{3,x}\, \mathrm{d}x = be_{313}[u_3(x_D) - u_3(x_C)] \tag{14}$$

where e_{313} is the piezoelectric stress constant of the sensor. If part of the sensor is debonded from the host beam, Eq. (14) is still valid.

By introducing the following notations:

$$\begin{aligned}
&\eta_i = \frac{\rho_i L^2}{E_2}, \quad \alpha_2 = \frac{h_2}{L}, \quad \beta_i = \frac{E_i}{E_2}, \quad \varphi_i = \frac{h_i}{h_2}, \quad \varphi_{vj} = \frac{h_{vj}}{h_2}, \quad \beta_{vj} = \frac{E_{vj}}{E_2} \quad (j = 1, 3) \\
&\xi = \frac{x}{L}, \quad u_{ni} = \frac{u_i}{h_2}, \quad w_{ni} = \frac{w_i}{h_2}, \quad T_{ni} = \frac{T_i}{E_2 b h_2}, \quad Q_{ni} = \frac{Q_i}{E_2 b h_2}, \quad i = 1, 2, 3 \\
&M_{ni} = \frac{M_i}{E_2 b h_2^2/12}, \quad t_n = \frac{t}{L^2}\sqrt{\frac{E_2 h_2^2}{12\rho_2}}, \quad V_n(t_n) = \frac{e_{311} V(t)}{E_2 h_2}
\end{aligned} \tag{15}$$

Eqs. (8)–(13) can be nondimensionalized as

$$\begin{aligned}
&m_1 k_t^2 \ddot{u}_{n1} = T_{n1,\xi} + \tau_{n1}, \quad m_1 k_t^2 \ddot{w}_{n1} = Q_{n1,\xi} + \sigma_{n1}, \quad m_1 \varphi_1^2 \alpha_1 k_t^2 \ddot{\psi}_1 = M_{n1,\xi} + 6\varphi_1 \tau_{n1} - \frac{12}{\alpha_2} Q_{n1} \\
&m_2 k_t^2 \ddot{u}_{n2} = T_{n2,\xi} - \tau_{n1} + \tau_{n2}, \quad m_2 k_t^2 \ddot{w}_{n2} = Q_{n2,\xi} - \sigma_{n1} + \sigma_{n2} \\
&m_2 \varphi_2^2 \alpha_2 k_t^2 \ddot{\psi}_2 = M_{n2,\xi} + 6\varphi_2(\tau_{n1} + \tau_{n2}) - \frac{12}{\alpha_2} Q_{n2}, \quad m_3 k_t^2 \ddot{u}_{n3} = T_{n3,\xi} - \tau_{n2} \\
&m_3 k_t^2 \ddot{w}_{n3} = Q_{n3,\xi} - \sigma_{n2}, \quad m_3 \varphi_3^2 \alpha_3 k_t^2 \ddot{\psi}_3 = M_{n3,\xi} + 6\varphi_3 \tau_{n2} - \frac{12}{\alpha_2} Q_{n3} \\
&T_{n1} = \beta_1 \alpha_1 u_{n1,\xi} - V_n, \quad T_{n2} = \beta_2 \alpha_2 u_{n2,\xi}, \quad T_{n3} = \beta_3 \alpha_3 u_{n3,\xi} \\
&M_{n1} = \beta_1 \varphi_1^2 \alpha_1 \psi_{1,\xi}, \quad M_{n2} = \beta_2 \varphi_2^2 \alpha_2 \psi_{2,\xi}, \quad M_{n3} = \beta_3 \varphi_3^2 \alpha_3 \psi_{3,\xi} \\
&\gamma_i = \alpha_2 w_{ni,\xi} + \psi_i, \quad \gamma_i = \frac{2c_i(1 + v_i)}{\beta_i \varphi_i} Q_{ni}, \quad i = 1, 2, 3 \\
&\tau_{n1} = k_1 r_{a1}\left[u_{n2} - u_{n1} - \frac{1}{2}(\varphi_1 \psi_1 + \varphi_2 \psi_2)\right] \\
&\tau_{n2} = k_2 r_{a2}\left[u_{n3} - u_{n2} - \frac{1}{2}(\varphi_2 \psi_2 + \varphi_3 \psi_3)\right] \\
&\sigma_{n1} = k_1 r_{a1}^e (w_{n2} - w_{n1}), \quad \sigma_{n2} = k_2 r_{a2}^e (w_{n3} - w_{n2})
\end{aligned} \tag{16}$$

where the double dot represents the second order derivation with respect to nondimensional time t_n, and the parameters are defined as

$$\begin{aligned}
&\alpha_i = \varphi_i \alpha_2, \quad m_i = \alpha_i \eta_i \ \ (i = 1, 2, 3), \quad \alpha_v = \varphi_v \alpha_2 \\
&k_v = \frac{1 - v}{(1 - 2v)(1 + v)}, \quad k_g = \frac{1}{2(1 + v)}, \quad r_{aj} = \frac{k_g \beta_{vj}}{\alpha_{vj}}, \quad r^e_{aj} = \frac{k_v \beta_{vj}}{\alpha_{vj}} \quad (j = 1, 2) \\
&k_t = \frac{1}{L^2}\sqrt{\frac{E_2 h_2^2}{12\rho_2}} = \sqrt{\frac{\alpha_2^3}{12 m_2}}
\end{aligned} \tag{17}$$

Substituting Eqs. (14), (2) and (3) into Eq. (7), the nondimensionalized control voltage becomes

$$V_n(t_n) = \sum_{i=1}^{N_c} g_{ni} y_{2i}(t_n) \tag{18}$$

where $y_{2i}(t_n)$ is the output of the ith MVO to the nondimensionalized charge input

$$q_n(t) = [u_{3n}(\xi_D) - u_{3n}(\xi_C)] \tag{19}$$

and g_{ni} are the nondimensional control gains given by

$$g_{ni} = \frac{g_i b e_{311} e_{313}}{E_2} \tag{20}$$

Denoting $\mathbf{Y}_1(\xi) = (u_{n1}, T^e_{n1}, w_{n1}, \psi_1, Q_{n1}, M_{n1})^{\mathrm{T}}$, $\mathbf{Y}_2(\xi) = (u_{n2}, T_{n2}, w_{n2}, \psi_2, Q_{n2}, M_{n2})^{\mathrm{T}}$, $\mathbf{Y}_3(\xi) = (u_{n3}, T^e_{n3}, w_{n3}, \psi_3, Q_{n3}, M_{n3})^{\mathrm{T}}$ and $\mathbf{Y} = (\mathbf{Y}_1^{\mathrm{T}}, \mathbf{Y}_2^{\mathrm{T}}, \mathbf{Y}_3^{\mathrm{T}})^{\mathrm{T}}$ in which $T^e_{ni} = T_{ni} + V_n(t)$ $(i = 1, 3)$, Eq. (16) can be rewritten into the following compact form:

$$\mathbf{Y}_{,\xi} = \mathbf{M}\ddot{\mathbf{Y}} + \widetilde{\mathbf{A}}\mathbf{Y} \quad \text{for beam with patches} \tag{21}$$

where $\mathbf{M} \in R^{18\times 18}$ is the mass matrix, $\widetilde{\mathbf{A}} \in R^{18\times 18}$ is the state matrix. Note that Eq. (21) is a set of homogeneous equations and the control items related to the voltage will appear in the boundary conditions of the piezoelectric actuator patches for uniformly distributed control voltage.

Similarly, the equation of motion of the host beam itself can also be rewritten as

$$\mathbf{Y}_{2,\xi} = \mathbf{M}_2\ddot{\mathbf{Y}}_2 + \widetilde{\mathbf{A}}_2\mathbf{Y}_2 \quad \text{for host beam} \tag{22}$$

where $\mathbf{M}_2 \in R^{6\times 6}$ is the mass matrix, $\widetilde{\mathbf{A}} \in R^{6\times 6}$ is the state matrix for the host beam.

The continuity conditions at the interfaces between the perfectly bonded and debonded regions are needed to ensure displacement continuity and force equilibrium. Therefore, all displacements and stress resultants at the interface should be continuous, as shown in Fig. 5, which can be expressed as

$$\mathbf{Y}(\xi_d^-) = \mathbf{Y}(\xi_d^+) \tag{23}$$

where ξ_d is the normalized coordinate of the interface.

The boundary conditions for the host beam and each piezoelectric patch should also be applied. For the host beam, its boundary conditions can be written in the following general form

$$\mathbf{D}_h^l \mathbf{Y}_2(0) + \mathbf{D}_h^r \mathbf{Y}_2(1) = \mathbf{D}_h, \quad \text{for } \forall t_n \tag{24}$$

where $\mathbf{D}_h^l \in R^{6\times 6}$, $\mathbf{D}_h^r \in R^{6\times 6}$ and $\mathbf{D}_h \in R^6$ are known matrices and vector corresponding to the given boundary conditions, $\mathbf{Y}_2(0)$ and $\mathbf{Y}_2(1)$ are the state vectors at both ends of the host beam. When the boundary conditions are homogeneous, $\mathbf{D}_h = 0$. The boundary conditions of the piezoelectric patches have the similar forms as described in Eq. (24). For instance, the boundary conditions of the ith piezoelectric actuator patch bonded on the upper surface of the host beam have the form

$$\mathbf{D}_{ai}^l \mathbf{Y}_1(\xi_{ai}^l) + \mathbf{D}_{ai}^r \mathbf{Y}_1(\xi_{ai}^r) = \mathbf{D}_{ai}, \quad \text{for } \forall t_n \tag{25}$$

where ξ_{ai}^{l} and ξ_{ai}^{r} are the nondimensionalized coordinates of the left and right ends of the actuator patch. For example, the matrices for free-free piezoelectric actuator patch with control voltage $V_n(t)$ are

$$\mathbf{D}_{a}^{l}=\begin{bmatrix}0&1&0&0&0&0\\0&0&0&0&1&0\\0&0&0&0&0&1\\0&0&0&0&0&0\\0&0&0&0&0&0\\0&0&0&0&0&0\end{bmatrix},\quad \mathbf{D}_{a}^{r}=\begin{bmatrix}0&0&0&0&0&0\\0&0&0&0&0&0\\0&0&0&0&0&0\\0&1&0&0&0&0\\0&0&0&0&1&0\\0&0&0&0&0&1\end{bmatrix},\quad \mathbf{D}_{a}=\begin{bmatrix}V_n\\0\\0\\V_n\\0\\0\end{bmatrix}=\begin{bmatrix}1\\0\\0\\1\\0\\0\end{bmatrix}V_n \tag{26}$$

Similarly, the boundary conditions of the ith sensor patch bonded on the lower surface have the form

$$\mathbf{D}_{si}^{l}\mathbf{Y}_1(\xi_{si}^{l})+\mathbf{D}_{si}^{r}\mathbf{Y}_1(\xi_{si}^{r})=\mathbf{D}_{si},\quad \text{for } \forall t_n \tag{27}$$

where the subscript 's' stands for sensor patches. If there is no mechanical and electrical loads applied on the boundary of the sensor patch, $\mathbf{D}_{si}=\mathbf{0}$.

4. Characteristic equation of the controlled beam with debonded piezoelectric patches

The eigenvalues of the closed loop system can be used to examine the sensitivity of the closed control system to the small debonding of the piezoelectric actuator patches. In this section, the characteristic equation is derived for the closed loop controlled beam with partly debonded piezoelectric patches. Without loss of generality, the derivation of the characteristic equation is given for the case that only one free–free piezoelectric pair is bonded on the host beam. Assume that the state vector can be separated in space and time as

$$\mathbf{Y}(\xi,t_n)=\overline{\mathbf{Y}}(\xi)\exp(\kappa t_n) \tag{28}$$

where $\overline{\mathbf{Y}}(\xi)$ is a function of spatial coordinate ξ, and κ is the eigenvalue. Substituting Eq. (31) into Eqs. (24) and (25), we have

$$\begin{aligned}&\overline{\mathbf{Y}}_{,\xi}(\xi)=\mathbf{A}(\kappa)\overline{\mathbf{Y}}(\xi)\quad \text{for beam with patches}\\&\overline{\mathbf{Y}}_{2,\xi}(\xi)=\mathbf{A}_2(\kappa)\overline{\mathbf{Y}}_2(\xi)\quad \text{for host beam}\end{aligned} \tag{29}$$

where $\mathbf{A}(\kappa)=\widetilde{\mathbf{A}}+\kappa^2\mathbf{M}$ and $\mathbf{A}_2(\kappa)=\widetilde{\mathbf{A}}_2+\kappa^2\mathbf{M}_2$. Eq. (29) becomes a set of ordinary differential equations with parameter κ, which is very complicated particularly for the debonding case.

Noting Eqs. (2) and (3), the control voltage in Eq. (18) can be transformed as

$$\overline{V}_n=\bar{q}_n\sum_{i=1}^{N_c}g_{ni}\overline{H}_i(\kappa) \tag{30}$$

where

$$\overline{H}_i(\kappa)=\frac{\kappa/\omega_{ci}}{[1+(\kappa/\omega_{ci})^2+2\zeta_{c1i}\kappa/\omega_{ci}][1+(\kappa/\omega_{ci})^2+2\zeta_{c2i}\kappa/\omega_{ci}]} \tag{31}$$

is the transfer function of the ith MVO in which ζ_{c1i}, ζ_{c2i} and ω_{ci} are its three parameters.

For different portions, the solutions of Eq. (29) can be written as follows

$$\begin{aligned}
&\overline{\mathbf{Y}}_2(\xi_A) = \mathbf{\Phi}_{OA}(\kappa)\overline{\mathbf{Y}}_2(0) \quad 0 < \xi \leqslant \xi_A \\
&\overline{\mathbf{Y}}(\xi_d^-) = \mathbf{\Phi}_{Ad}(\kappa)\overline{\mathbf{Y}}(\xi_A) \quad \xi_A < \xi < \xi_d^- \\
&\overline{\mathbf{Y}}(\xi_B) = \mathbf{\Phi}_{dB}(\kappa)\overline{\mathbf{Y}}(\xi_d^+) \quad \xi_d^+ < \xi < \xi_B \\
&\overline{\mathbf{Y}}_2(\xi_C) = \mathbf{\Phi}_{BC}(\kappa)\overline{\mathbf{Y}}_2(\xi_B) \quad \xi_B < \xi < \xi_C
\end{aligned} \tag{32}$$

where $\mathbf{\Phi}_{OA} \in R^{6\times 6}$, $\mathbf{\Phi}_{Ad} \in R^{18\times 18}$, $\mathbf{\Phi}_{dB} \in R^{18\times 18}$ and $\mathbf{\Phi}_{BC} \in R^{6\times 6}$ are transition matrices. The continuity and boundary conditions become

$$\begin{aligned}
&\overline{\mathbf{Y}}_2(\xi_A) = [\mathbf{0}_6 \quad \mathbf{I}_6 \quad \mathbf{0}_6]\overline{\mathbf{Y}}(\xi_A) \quad \text{at } \xi = \xi_A \\
&\overline{\mathbf{Y}}(\xi_d^-) = \overline{\mathbf{Y}}(\xi_d^+) \quad \text{at } \xi = \xi_d \\
&\overline{\mathbf{Y}}_2(\xi_B) = [\mathbf{0}_6 \quad \mathbf{I}_6 \quad \mathbf{0}_6]\overline{\mathbf{Y}}(\xi_B) \quad \text{at } \xi = \xi_B \\
&\mathbf{D}_h^l\overline{\mathbf{Y}}_2(0) + \mathbf{D}_h^r\overline{\mathbf{Y}}_2(1) = 0 \quad \text{host beam} \\
&\mathbf{D}_a^l\overline{\mathbf{Y}}_1(\xi_A) + \mathbf{D}_a^r\overline{\mathbf{Y}}_1(\xi_B) = \mathbf{D}_a \quad \text{actuator patch} \\
&\mathbf{D}_s^l\overline{\mathbf{Y}}_3(\xi_A) + \mathbf{D}_s^r\overline{\mathbf{Y}}_3(\xi_B) = 0 \quad \text{sensor patch}
\end{aligned} \tag{33}$$

Substituting Eqs. (19) and (30) into Eq. (26), the vector $\mathbf{D}_a$ can be expressed as

$$\mathbf{D}_a = \mathbf{B}[\overline{\mathbf{Y}}(\xi_B) - \overline{\mathbf{Y}}(\xi_A)] \tag{34}$$

where

$$\mathbf{B} = \left[\sum_{i=1}^{N_c} g_{ni}\overline{H}_i(\kappa)\right]\begin{bmatrix}1\\0\\0\\1\\0\\0\end{bmatrix}[0\ \ 0\ \ 0\ \ 0\ \ 0\ \ 0\ \ 0\ \ 0\ \ 0\ \ 0\ \ 0\ \ 0\ \ 0\ \ 1\ \ 0\ \ 0\ \ 0\ \ 0\ \ 0] \tag{35}$$

is a 6×18 matrix. Therefore Eq. (33) will become a set of homogeneous equations by moving the control term $\mathbf{D}_a$ to the left side of the equations.

Combining Eqs. (32)–(34), the equations can be rewritten into the following form

$$\mathbf{R}(\kappa)\mathbf{Z} = \mathbf{0} \tag{36}$$

where

$$\mathbf{R}(\kappa) = \begin{bmatrix}
\mathbf{\Phi}_{OA} & -\mathbf{I}_6 & \mathbf{0} & \mathbf{0} & \mathbf{0} & \mathbf{0} & \mathbf{0} & \mathbf{0} \\
\mathbf{0} & \mathbf{I}_6 & [\mathbf{0}_6 \ -\mathbf{I}_6 \ \mathbf{0}_6] & \mathbf{0} & \mathbf{0} & \mathbf{0} & \mathbf{0} & \mathbf{0} \\
\mathbf{0} & \mathbf{0} & \mathbf{\Phi}_{Ad} & -\mathbf{I}_{18} & \mathbf{0} & \mathbf{0} & \mathbf{0} & \mathbf{0} \\
\mathbf{0} & \mathbf{0} & \mathbf{0} & \mathbf{I}_{18} & -\mathbf{I}_{18} & \mathbf{0} & \mathbf{0} & \mathbf{0} \\
\mathbf{0} & \mathbf{0} & \mathbf{0} & \mathbf{0} & \mathbf{\Phi}_{dB} & -\mathbf{I}_{18} & \mathbf{0} & \mathbf{0} \\
\mathbf{0} & \mathbf{0} & \mathbf{0} & \mathbf{0} & \mathbf{0} & [\mathbf{0}_6 \ \mathbf{I}_6 \ \mathbf{0}_6] & -\mathbf{I}_6 & \mathbf{0} \\
\mathbf{0} & \mathbf{0} & \mathbf{0} & \mathbf{0} & \mathbf{0} & \mathbf{0} & \mathbf{\Phi}_{BC} & -\mathbf{I}_6 \\
\mathbf{0} & \mathbf{D}_a^l & \mathbf{B} & \mathbf{0} & \mathbf{0} & -\mathbf{B} & \mathbf{D}_a^r & \mathbf{0} \\
\mathbf{0} & \mathbf{D}_s^l & \mathbf{0} & \mathbf{0} & \mathbf{0} & \mathbf{0} & \mathbf{D}_s^r & \mathbf{0} \\
\mathbf{D}_h^l & \mathbf{0} & \mathbf{0} & \mathbf{0} & \mathbf{0} & \mathbf{0} & \mathbf{0} & \mathbf{D}_h^r
\end{bmatrix} \tag{37}$$

$$\mathbf{Z} = [\overline{\mathbf{Y}}_2^T(0), \overline{\mathbf{Y}}_2^T(\xi_A), \overline{\mathbf{Y}}^T(\xi_A), \overline{\mathbf{Y}}^T(\xi_d^-), \overline{\mathbf{Y}}^T(\xi_d^+), \overline{\mathbf{Y}}^T(\xi_B), \overline{\mathbf{Y}}_2^T(\xi_b), \overline{\mathbf{Y}}_2^T(1)]^T$$

in which $\mathbf{I}_6$ and $\mathbf{I}_{18}$ represents 6×6 and 18×18 identity matrices respectively.

Eq. (36) is a set of simultaneous homogeneous algebraic equations, which possess a nontrivial solution only if the determinant of the coefficient matrix $\mathbf{R}(\kappa)$ is zero, i.e.

$$\det[\mathbf{R}(\kappa)] = 0 \tag{38}$$

Eq. (38) is the characteristic equation for the closed loop control system, which can give infinite number of eigenvalues of the controlled beam. It should be pointed out that using Eq. (38) directly to find the eigenvalues may encounter difficulty in computation because the very thin adhesive layers between the piezoelectric patches and the host structure make some entries in the coefficient matrix $\mathbf{R}(\kappa)$ extremely large. To solve this problem, the beam should be divided into several small elements so that all the entries of the transition matrices between the adjacent dividing points are within a proper range. However, unlike the FEM, the eigenvalues obtained from the given scheme is not dependent on the number of elements.

The eigenvalues are complex for a controlled system, which give the information of active damping and frequency for each vibration mode. It is clear from Eq. (28) that all eigenvalues of a stable control system should have negative real parts. If denote

$$\kappa_i = n_i + \Omega_{\mathrm{d}i} I \tag{39}$$

where n_i is the active damping coefficient, $\Omega_{\mathrm{d}i}$ is the nondimensional frequency of the actively damped beam, the damping ratio for the ith mode can be estimated by

$$\zeta_{\mathrm{a}i} = -\frac{\mathrm{sgn}(n_i)}{\sqrt{1 + (\Omega_{\mathrm{d}i}/n_i)^2}} \tag{40}$$

The physical frequency can be obtained by

$$\omega_{\mathrm{d}i} = k_t \Omega_{\mathrm{d}i} \tag{41}$$

If the active damping ratio for a given mode is positive, the closed loop control provides an effect damping to this mode.

5. Experimental implementation and validation

To validate the theoretical model and solution method, the first experiment for active vibration control of beams using lead zirconate titanate (PZT) patches is designed and performed using four specimens. As shown in Fig. 5, on the surfaces of each specimen one PZT-51 patch pair is bonded as the actuator pair, and another pair is used as the sensor. Table 1 lists the material properties and geometrical dimensions of all the specimens. An edge debonding at the left end of one patch in the actuator pair is introduced using 0.02-mm-

Table 1
Material properties and geometrical dimensions of test specimens

Item	Host beam	Piezoelectric patch	Adhesive layer
Material	5000 series aluminum	PZT-51	Super glue
Mass density, kg/m^3	2700	7700	
Young's modulus, GPa	69	70	2.4
Poisson's ratio	0.3	0.3	0.34
Capacitance, pF	–	41,220	–
Piezo-constant e_{31}, m/V	–	9.3	–
Thickness, mm	0.89	0.5	0.15
Length, m	0.6	0.04	0.04
Width, m	0.03	0.03	0.03

thick Teflon film. All the PZT patches are bonded perfectly in specimen 1. The debonding lengths of the actuator patches are 0.5, 1.0 and 1.5 cm in specimen 2, 3 and 4 respectively. Each specimen is clamped at its left end and free at the other. The distance between the left ends of the actuator pair and the clamped end is 1 cm, and that of the sensor patches is 8 cm. In the experiment, only one of the sensor patches is used as the sensor.

Fig. 6 depicts the test setup for the active control test of aluminum beam. The equipment used includes a National Instruments Signal conditioner, PI E-507.00 HVPZT power amplifier (three channels, gain $g_p = 100$) and a computer with a data acquisition system. A Polytec CLV-1000 Laser vibrometer and a Tektronix 465 oscilloscope are also used to monitor the vibration of the specimens. Based on LabView graphical programming platform, an active control program is developed using the MVO. After the sensor signal is put into the signal conditioner and read by the computer, a proper control voltage is generated by the control program according to the control law. After amplified by the power amplifier, the control voltage is fed back to the actuator patches to perform closed loop control of the specimens, as shown in Fig. 6(b).

The first three frequencies of the specimens measured in the test are listed in Table 2, and the theoretical ones are also given. In general, the measured frequencies correlate reasonably to the theoretical ones. The natural damping ratios for the first three modes of specimen 1 are measured as 0.0045, 0.0013 and 0.001 respectively. To control the first three modes of each specimen, three MVOs are designed and used in the control software. In the three MVOs, the three natural frequencies (2.45, 13.5 and 34.6 Hz) are used

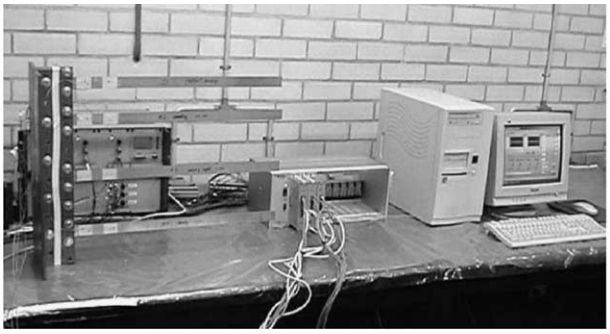

(a)

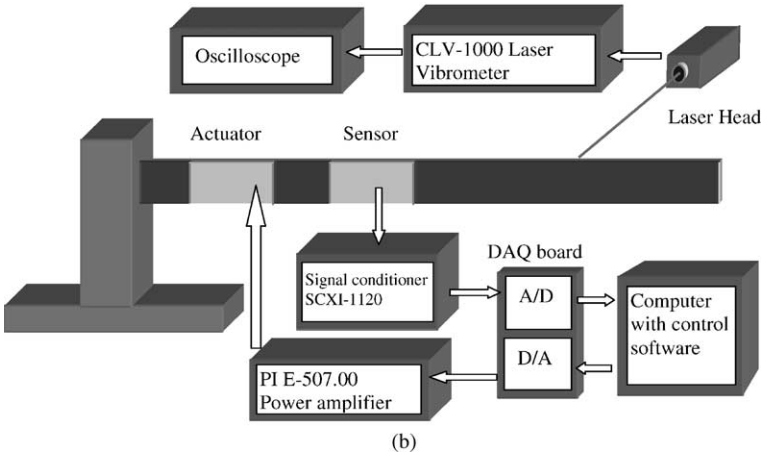

(b)

Fig. 6. Experiment setup: (a) photo of the overall experimental setup and (b) block diagram of the active control test.

Table 2
The first three measured and theoretical frequencies of specimens (Hz)

Mode no.	Specimens							
	Specimen 1 (debonding length: 0 mm)		Specimen 2 (debonding length: 5 mm)		Specimen 3 (debonding length: 10 mm)		Specimen 4 (debonding length: 15 mm)	
	Test	Theory	Test	Theory	Test	Theory	Test	Theory
1st frequency	2.45	2.46	2.44	2.46	2.45	2.45	2.42	2.44
2nd frequency	13.5	13.94	13.6	13.86	13.7	13.81	13.3	13.75
3rd frequency	34.6	35.22	34.4	34.98	34.8	34.83	33.9	34.72

respectively, and big damping ratios, $\xi_{c1} = 0.5$ and $\xi_{c2} = 0.65$, are used in order to make the control more robust. In the test, by using a negative control gain, the designated mode can be excited. After switching off the excitation for a while, active control is turned on to control this mode. Note that except the expected

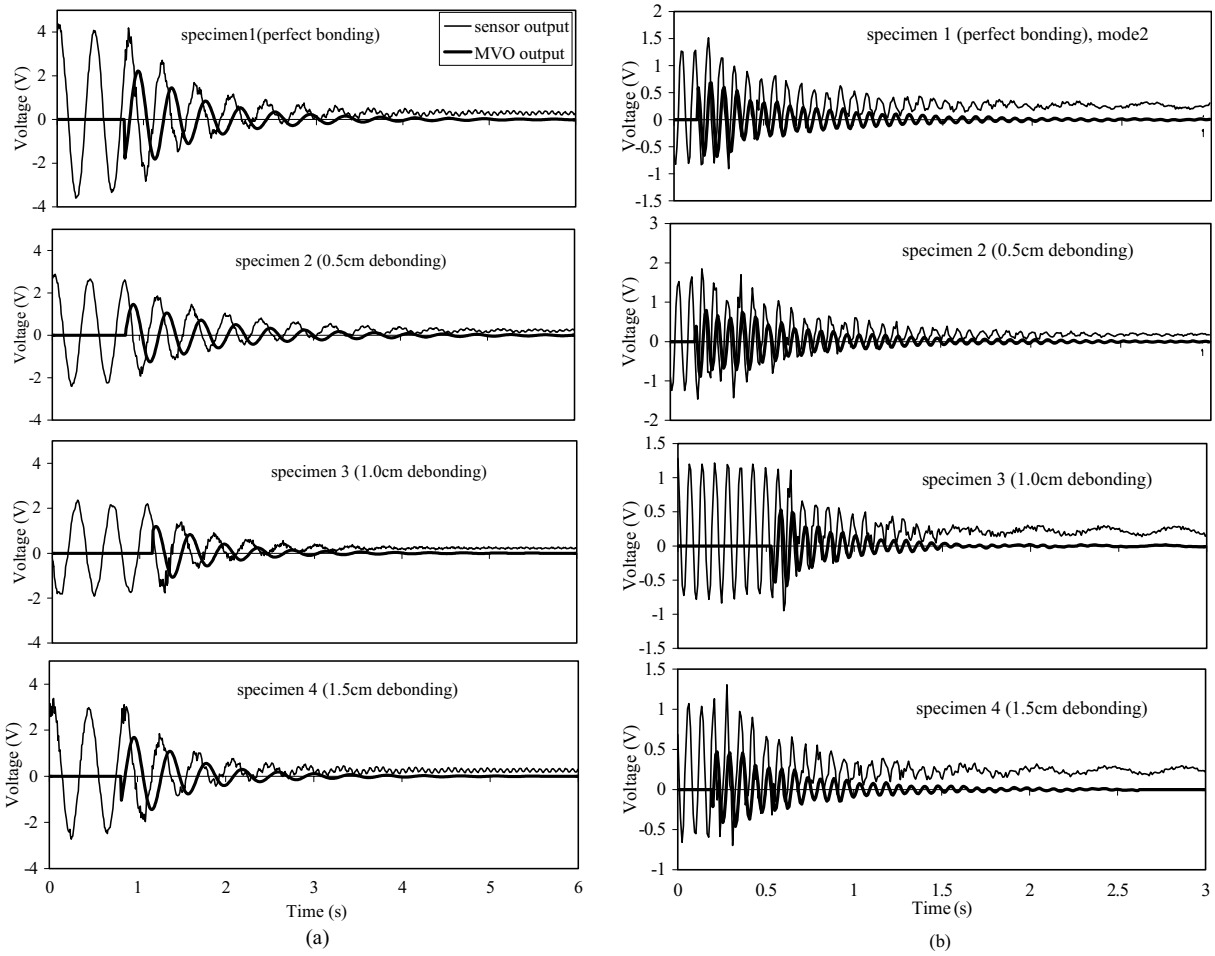

Fig. 7. (a) Mode 1: sensor and MVO outputs for the controlled modes in experiment; (b) Mode 2: sensor and MVO outputs for the controlled modes in experiment (continued); (c) Mode 3: sensor and MVO outputs for the controlled modes in experiment (continued).

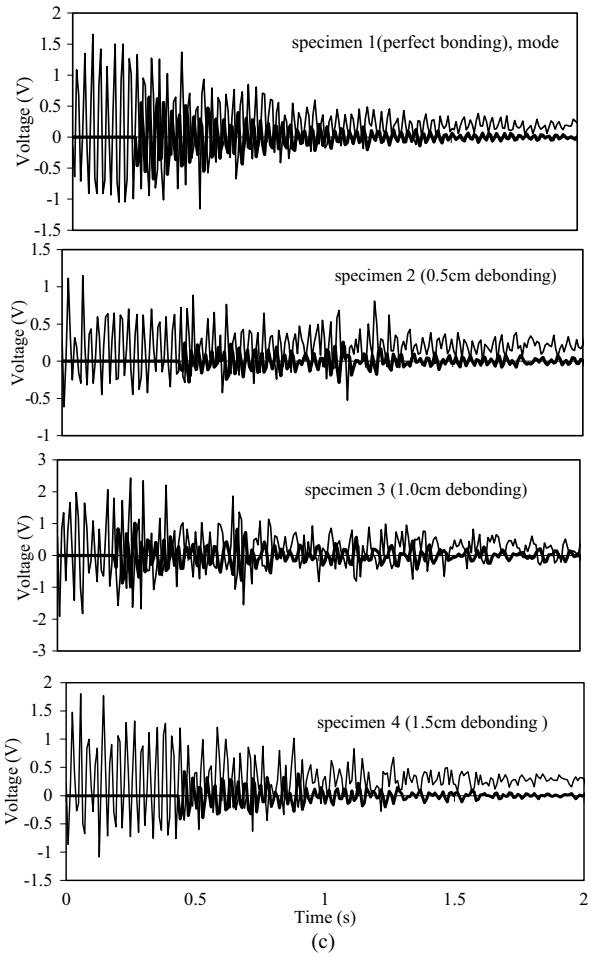

(c)

Fig. 7 (*continued*)

mode, other vibration modes can also be slightly excited by switching on and off of the actuating voltage. Fig. 7 presents the outputs of the sensor and the MVOs in the experiment of the closed loop control for the four specimens. The real control voltage applied on the actuator patches can be obtained by multiplying the MVO's output by 100, the gain of the voltage amplifier. Fig. 7 shows that the first three modes of the beam can be effectively controlled by the MVO. It can bee seen that each MVO with relatively large damping ratios can successfully extract the designated modal velocity from the sensor output even when large debondings of the actuator patches occur. Therefore, the MVO can be used in both damage detection and active vibration control of structures by properly adjusting its damping ratios.

To compare the test results and the theoretical ones, the control gain in the experiment should be determined first. The output voltage of the sensor patch can be obtained by

$$V_s(t) = q(t)/C \tag{42}$$

where C is the capacitance of the sensor patch. Noting the linearity of the observers in Eqs. (2) and (3), the control gain in the experiment is g_p/C, i.e. $g = 100/(41,220 \times 10^{-12}) = 2.43 \times 10^9$. The nondimensional

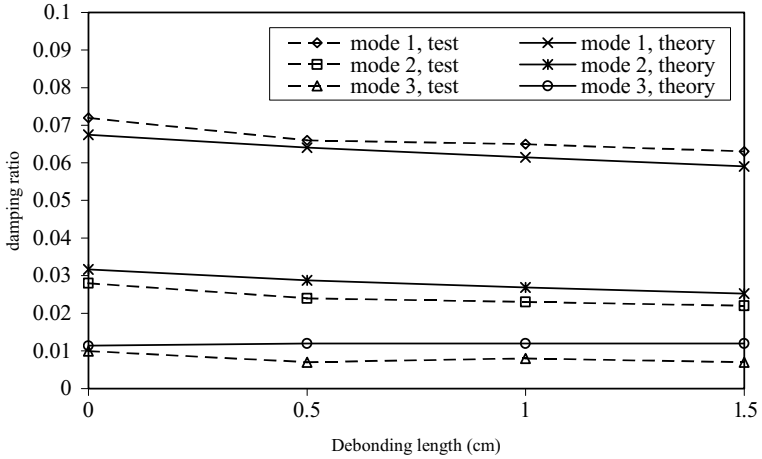

Fig. 8. Damping ratios for the first three modes: perfectly bonded specimen, debonding length of 0.5 cm, debonding length of 1.0 cm.

control gain can be calculated as 0.094. The damping ratios for the first three modes of the four specimens obtained by both experiment and simulation are plotted in Fig. 8. Fig. 8 shows that the damping ratios obtained by theory are in a good agreement with those measured in the experiment. For example, for the four specimens, theoretical damping ratios of the first mode are 0.0675, 0.06404, 0.06149 and 0.05903 respectively, and those measured in the experiment are 0.072, 0.066, 0.065 and 0.063, the relative errors are less than 7%. For the first mode, the measured damping ratios are slightly larger than the theoretically predicted ones because the natural damping is not considered in the theoretical calculation. However, it is noted that the test damping ratios for the second and third modes are smaller than theoretical ones. This is probably because the relatively low sampling rate (125 Hz) in the control loop affects the control efficiency of mode 2 and mode 3. In addition, the active control of higher modes may be affected more easily than that of the first mode by factors such as phase lag and external disturbances.

In the second test, we designed a sensitive controller for the first vibration mode based on the MVO as described in Section 2 to detect debonding in the specimens used in the first test. Firstly, we deliberately adjusted the controller to a critical condition (oscillation) for specimen 1 with perfectly bonded actuators. To this end, the natural frequency and damping ratios are selected as $\omega_c = 2\pi \times 2.4$ rad/s and $\zeta_{c1} = \zeta_{c2} = 0.02$, respectively, and the control gain is taken as $g = 0.0016 \times 100/(41,220 \times 10^{-12}) = 3881610.9$. The closed-loop response of the controlled beam to a disturbance is shown in Fig. 9a. It can be seen that the vibration amplitude of the controlled beam subjected to a transient loading almost keep unchanged, which indicates that the controlled beam is critically stable. It is expected that a small frequency change cause by a debonding may destabilize the unrobust control. Then the same sensitive controller was applied to specimen 2 and 3 respectively without changing any parameters in the controller and the MVO. The responses of specimen 2 and 3, controlled by the sensitive controller defined in specimen 1, to an external transient loading are shown in Fig. 9b and c respectively. Clearly, the small frequency difference between specimen 1 and 2 (or specimen 3) caused by the debonding makes the closed loop control unstable. It is easy to qualitatively identify the presence of debonding from the rapidly increasing amplitude of the specimens. This test shows that the present detect methodology can pick up small frequency change due to the amplifying effect of the deliberately designed sensitive controller based on MVO.

It is worth pointing out that the above detection test of debonding using different specimens may not be absolutely accurate. This is because the second test aims to experimentally verify the detection method of a frequency shift due to change in only one structural parameter, e.g., debonding. Due to limited manu-

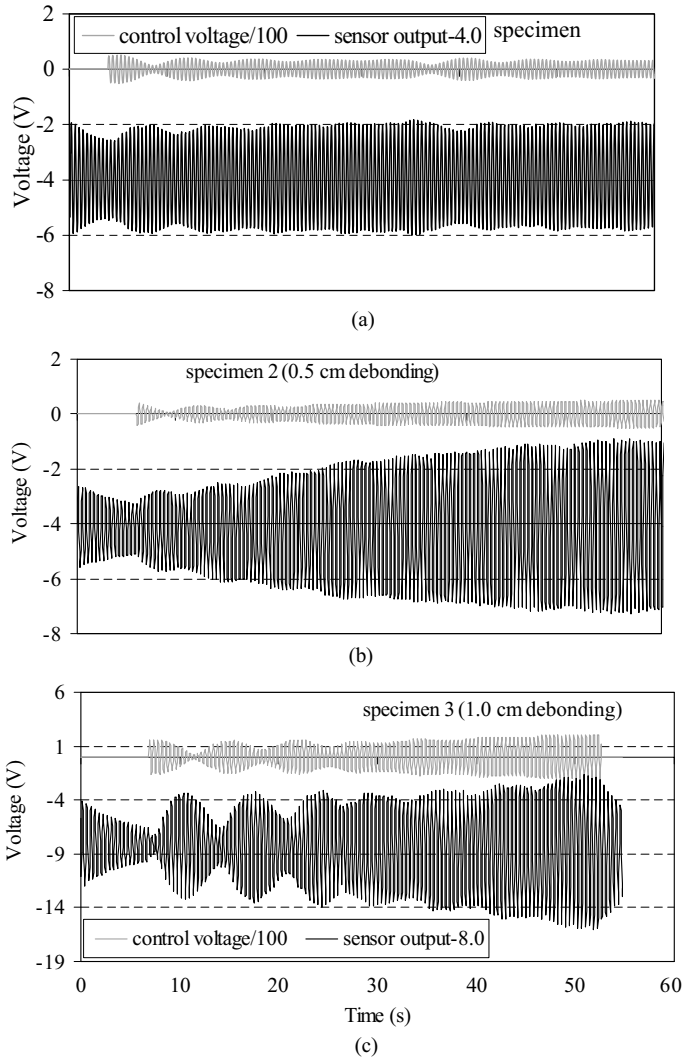

Fig. 9. Response of the sensitive control system to actuator debonding: (a) perfectly bonded specimen, (b) debonding length of 0.5 cm and (c) debonding length of 1.0 cm.

facturing facilities, it is extremely difficult, if not impossible, to artificially introduce the debonding as the only change to the same specimen system parameters. Therefore, in addition to the introduced debonding, there may be other parameters, such as manufacturing tolerance and support condition, present that may also contribute to the frequency shift.

The third test is designed to demonstrate the effectiveness and practicality of the detection method using the sensitive controller in terms of identifying frequency changes caused by an attached concentrated mass, rather than stringently realizing debonding as the only one parameter change. A sensitive MVO controller is designed for specimen 1 and the parameters in the controller are the same as test two so that the active control of specimen 1 is in a critical status. In this case, the closed loop control of the beam is tailored very sensitive to frequency changes. When two small mass patches of 2 mm are attached at the free end of the specimen using double-sided adhesive tapes, the slight change in its fundamental frequency is even not

noticeable using our equipment. However, this slight frequency change caused by the mass attachment can be easily detected by the increasing vibration amplitude since it makes the active control unstable. The attachment of two mass patches of 3 mm decreases the frequency to 2.43 Hz approximately, and it also destabilizes the control system, as shown in Fig. 10.

The experiment demonstrated the concept of active detection of small damage in structures using a deliberately designed sensitive MVO controller. Even a small frequency change due to structural damage, after amplified by the sensitive controller, will destabilize the controlled structure, and consequently, it can be easily determined by observing the increasing vibration amplitude. In practice, the instability of a controlled structure may be not acceptable. A possible way of applying this detection concept is that the controller starts the sensitive "detection mode" for a short period at a pre-selected interval, and it operates in the robust mode in most of the time. Another possible way of using this concept is that the detection procedure is performed on a virtue system whose parameters are measured in real-time from true structure. In addition, since control failure of an unrobust controller may be caused by several other factors in addition to the structural damages. In this case, actuator debonding is only one of the possible reasons for

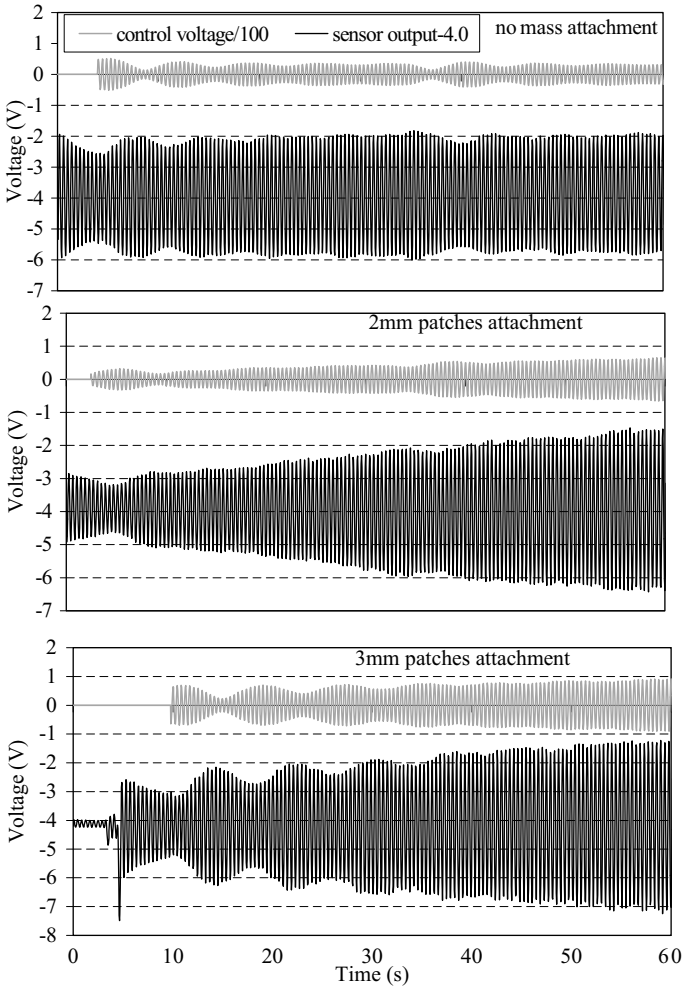

Fig. 10. Response of the sensitive control system to small patch attachments.

control destabilization, and therefore, other factors should be also carefully checked before a final detection conclusion is drawn.

6. Illustrative examples and analysis

As an illustrative example, consider a cantilevered host beam with two pairs of piezoelectric patches, shown in Fig. 5. The left piezoelectric patch pair, 4/60 long and located 1/60 from its left end to the clamped end of the beam, is used as the actuator pair. The right piezoelectric pair, which is also 4/60 long and located 5/60 from its left end to the clamped end, serves as sensors. In this example, only the upper one in the sensor pair is used as the sensor. The parameters used in the example are: $v_1 = v_2 = v_3 = 0.3$, $v_{v1} = v_{v3} = 0.34$, $\alpha_2 = 1/600$, $\beta_1 = \beta_3 = 0.9$, $\beta_{v1} = \beta_{v3} = 24/700$, $\eta_1 = \eta_3 = 3.9 \times 10^{-8}$, $\eta_2 = 1.39 \times 10^{-8}$, $\varphi_1 = \varphi_3 = 0.5$, $\varphi_{v1} = \varphi_{v3} = 0.15$, $(\beta_2 = \varphi_2 \equiv 1)$.

Firstly, to perform active control of the beam using the MVO given in Eq. (7), the natural frequencies of the beam should be calculated. Table 3 presents the first 10 eigenvalues of the open loop beam, which gives the first 10 natural frequencies of the beam. Compared with the host beam itself, the bonded piezoelectric patches on the host beam increases its first two modal frequencies remarkably and decreases its third to tenth modal frequencies to different extent.

Table 3
The first 10 eigenvalue pairs of the open loop beam

	Beam with piezo-patches	Host beam only
κ_1	$\pm 4.2598i$	$\pm 3.5160i$
κ_2	$\pm 24.1919i$	$\pm 22.0342i$
κ_3	$\pm 61.5957i$	$\pm 61.6955i$
κ_4	$\pm 115.4765i$	$\pm 120.8957i$
κ_5	$\pm 192.1925i$	$\pm 199.8431i$
κ_6	$\pm 288.6486i$	$\pm 298.5196i$
κ_7	$\pm 397.5756i$	$\pm 416.9218i$
κ_8	$\pm 526.6086i$	$\pm 555.0445i$
κ_9	$\pm 688.5980i$	$\pm 712.8815i$
κ_{10}	$\pm 881.7859i$	$\pm 890.4261i$

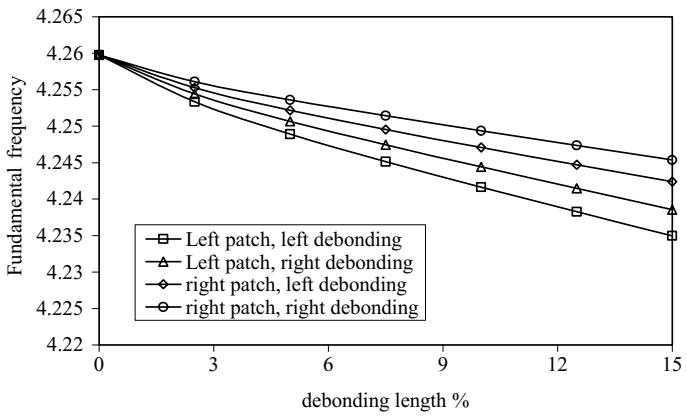

Fig. 11. Fundamental frequency versus length and location of edge debonding in actuator patches.

When an edge debonding occurs between the piezoelectric actuator patch and the host beam, the frequencies of the smart beam change. For the uncontrolled beam, the fundamental frequency will slightly change with the debonding length and debonding locations, as shown in Fig. 11. In Fig. 11, the effects of the edge debondings with different lengths introduced in the upper actuator patch on the fundamental frequency are given. It can be seen from Fig. 11 that an edge debonding of the piezoelectric patch will lead to a reduction of the fundamental frequency of the beam. When the edge debonding is closer to the clamped end of the beam, it decreases the fundamental frequency more remarkably. However, the frequency change caused by a small debonding is very small. For example, a 2.5% edge debonding at the left end of the left piezoelectric patch results in a 0.15% reduction of the fundamental frequency. Detection of such a small frequency change can be quite difficult if not impossible.

Secondly, the closed loop control of the beam with perfectly bonded piezoelectric actuator patches should be performed. In general, the higher order controlled modes are much more sensitive to the debonding of the piezoelectric than the lower order modes. For example, when a beam is controlled by a collocated piezoelectric actuator/sensor pair, the higher order modes are easily destabilized by the actuator debonding (Sun and Tong, 2002). However, in practice, the higher order modes are not easy to be controlled and they are more likely affected by uncertainties, and the detection based on which may not be reliable. Therefore, in order to detect small debonding of the piezoelectric patches by closed loop control, the control system should be made as simple as possible and the control effect should be easily observed. To this end, we aim at detecting the debonding of the piezoelectric patches by controlling the first mode of the beam only. When using the MVO (2) and (3) to control the first mode, the frequencies in both observers are chosen to be equal to the fundamental natural frequency (i.e. 4.26) of the beam. In this example, the same damping ratios in the two observers are used, i. e. $\zeta_c = \zeta_{c1} = \zeta_{c2}$.

The active damping ratio for the controlled mode depends on the control gain and the damping ratios used in the observers, as shown in Fig. 12. When closed loop control provides positive active damping ratio to the controlled mode, the controlled mode is stable. If the active damping ratio is negative, the controlled mode becomes unstable. For detection purpose, the control system should be designed stable in the perfect bonding case. On the other hand, the control system should be sensitive enough to detect small frequency change of the system, which requests that the active damping ratio should be very small, as indicated in Fig. 3. To this end, we choose the damping ratio in the observers as 0.02, and take the nondimensional control as 5×10^{-5}. In this case, when the piezoelectric actuator patches are perfectly bonded on the host beam, the first eigenvalue of the controlled beam is $-0.000043 + 4.175i$ which has a negative real part and hence the

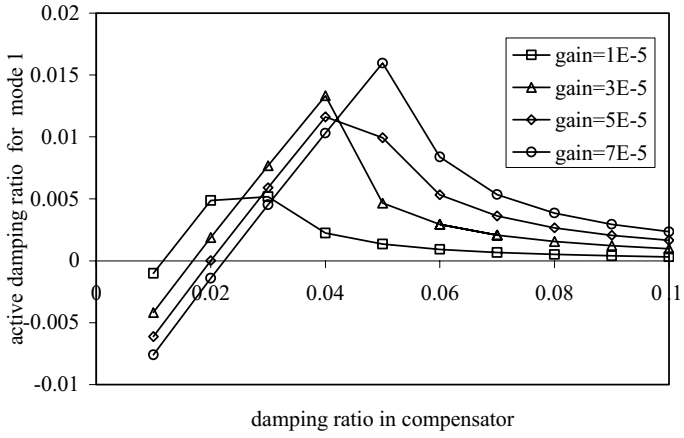

Fig. 12. Effect of versus damping ratio in compensator and control gain on active damping.

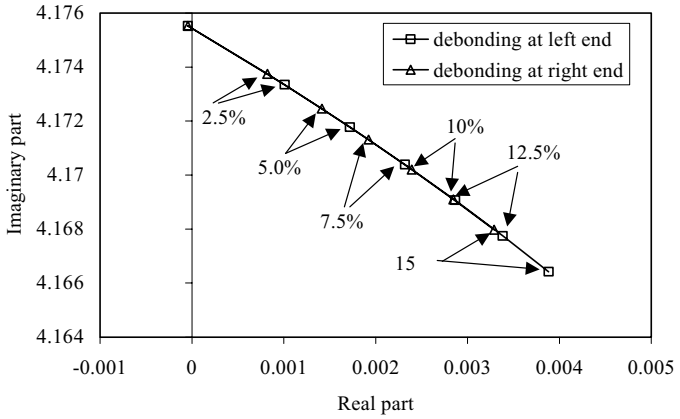

Fig. 13. Root loci for mode 1 with different debonding lengths at left and right ends of the upper actuator patch.

control of the first modes is stable. However, the active damping ratio for the first mode is 0.001%, which means the closed control is very sensitive.

Thirdly, the edge debondings of the upper actuator patch are to be detected by the deliberately designed sensitive control system. To this end, place an edge debonding of 2.5%, 5%, 7.5%, 10%, 12.5% and 15% of the original length at the both ends of the upper actuator patch respectively, the first eigenvalue of the closed loop system are calculated from Eq. (38). For different locations of the debonding, the root loci of the controlled system are presented in Fig. 13 as the debonding length changes. In this figure, all root loci start from the point $(-0.000043 + 4.175i)$ near the imaginary axis but on the left plane, which indicates that the designed control system is stable but sensitive for the perfect bonding case. As the debonding length increases, the real part of the eigenvalue increases too and the root loci enter into the right half plane. For example, a 2.5% debonding at the left end of the upper actuator patch alters the first eigenvalue from $-0.000043 + 4.175i$ to $0.001 + 4.173i$, which makes the control of the first mode unstable. The similar trend of the root loci with the different length of the debonding at the right end of the actuator patch can be observed. However, the debonding with same length at the right end of the actuator causes less change of the first eigenvalue than that at the left end.

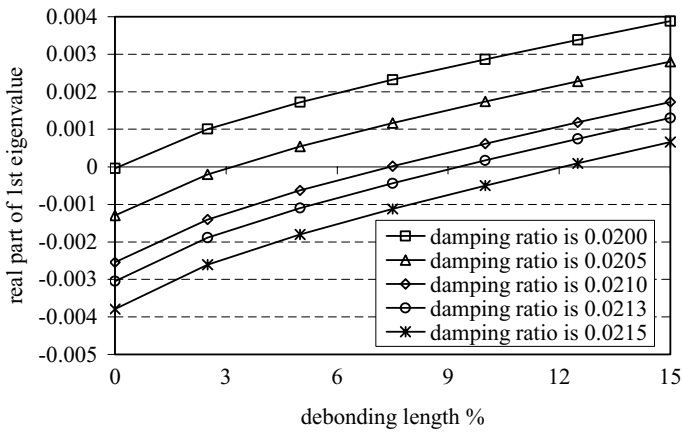

Fig. 14. Effect of damping ratio in the MVO on sensitivity of the control system to actuator debonding.

Since the process from stable to unstable state can lead to a rapid increasing of the vibration amplitude, it is easy to be observed, and hence a small debonding of the actuator patch can be easily detected. Fig. 13 shows that a very small debonding in the upper piezoelectric actuator patch can destabilize the controlled mode and consequently can be detected using the sensitive closed loop control system.

Fourthly, we estimate the debonding length of the actuator patch by designing control system with different sensitivities. The sensitivity of the control system to the debonding of the actuator patch is determined by the control gain and the damping ratios in the MVO. When the damping ratio in the modal velocity varies slightly, the maximum debonding length that the control system can tolerate is also changed. For example, when the control gain is 5×10^{-5} and the damping ratio is 0.0215, the control system can tolerate a 10% edge debonding of the actuator patches, whereas it can only endure a 5% debonding when the damping ratio is 0.0205, as shown in Fig. 14. In other words, if the first mode controlled by the MVO with damping ratio 0.0205, it becomes unstable only when the debonding length is larger than 5%. Similarly, if the damping ration in MVO is 0.0215, the control collapses only when the debonding length is larger than 10%. In such a way, the debonding length of the actuator patch can be estimated using control system with different sensitivities.

7. Conclusion

A practical active control based detection scheme is presented to identify small frequency shift caused by small damages in a controlled structure. A MVO is designed to perform active vibration control of beams using piezoelectric actuator/sensor patches. By properly choosing the parameters in the MVO, the closed loop control system can be made sensitive to small frequency change. In order to apply this method to detect debonding of piezoelectric patches on a smart beam, a detailed model of beam with partly debonded piezoelectric patches is established based and a characteristic equation is also derived. The established mathematical model, the obtained eigenvalues and the MVO are validated by experiment and good agreement between experimental and theoretical results is observed. The simulation example shows that the active control based detection method is effective in detecting small actuator debonding. It is found that even a debonding whose length is only 0.1% of the entire beam can destabilize the designed sensitive control system, and thus it can be detected.

Acknowledgements

The authors are grateful to the support of the Australia Research Council through a Large Grant (Grant No. A10009074). The authors would also like to thank the anonymous reviewers for their valuable suggestions on refining the detection experiment.

References

Beard, S., Chang, F.K., 1997. Active damage detection in filament wound composite tubes using built-in sensors and actuators. Journal of Intelligent Material Systems and Structures 8 (10), 891–897.

Fukunaga, H., Hu, N., Chang, F.K., 2002. Structural damage identification using piezoelectric sensors. International Journal of Solids and Structures 39 (2), 393–418.

Islam, A.S., Cralg, 1994. Damage detection in composite structures using piezoelectric materials. Smart Materials and Structures 3, 318–328.

Jian, X.H., Tzou, H.-S., Lissenden, C.J., et al., 1997. Damage detection by piezoelectric patches in a free vibration method. Journal of Composite Materials 31 (4), 345–359.

Lee, C.K., Moon, F.C., 1990. Modal sensors/actuators. Journal of Applied Mechanics 57 (2), 434–441.
Ray, L.R., Tian, L., 1999. Damage detection in smart structures through sensitivity enhancing feedback control. Journal of Sound and Vibration 227 (5), 987–1002.
Ray, L.R., Koh, B.H., Tian, L., 2000. Damage detection and vibration control in smart plates: towards multifunctional smart structures. Journal of Intelligent Materials Systems and Structures 11 (9), 725–739.
Seeley, C.E., Chattopadhyay, A., 1999. Modeling of adaptive composites including debonding. International Journal of Solids and Structures 36 (12), 1823–1843.
Sun, D.C., Tong, L., 2001. Modal control of smart shells by optimized discretely distributed piezoelectric transducers. International Journal of Solids and Structures 38 (18), 3281–3299.
Sun, D.C., Tong, L., 2002. Control stability analysis of smart beams with debonded piezoelectric actuator layer. AIAA Journal 40 (9), 1852–1858.
Sun, D.C., Wang, D.J., Xu, Z.L., 1999. Distributed piezoelectric element method for vibration control of smart plates. AIAA Journal 37 (11), 1459–1463.
Sun, D.C., Tong, L., Atluri, S.N., 2001. Effects of piezoelectric sensor/actuator debonding on vibration control of smart beams. International Journal of Solids and Structures 38 (50–51), 9033–9051.
Tong, L., Sun, D.C., Atluri, S.N., 2001. Sensing and actuating behaviors of piezoelectric layers with debonding in smart beams. Smart Materials and Structures 10 (4), 713–723.
Tylikowski, A., 2001. Effects of piezoactuator delamination on the transfer functions of vibration control systems. International Journal of Solids and Structures 38 (10–13), 2189–2202.
Xiao, H., Bruhns, O.T., Waller, H., et al., 2001. An input/output-based procedure for fully evaluating and monitoring dynamic properties of structural systems via a subspace identification method. Journal of Sound and Vibration 246 (4), 601–623.
Zou, Y., Tong, L., Steven, G.P., 2000. Vibration-based model-dependent damage (delamination) identification and health monitoring for composite structures—A review. Journal of Sound and Vibration 230, 357–378.